Experimental Solid–Liquid Mass Transfer around Free-Moving Particles in an Air-Lift Membrane Bioreactor with Optical Techniques

Naila Bouayed, Manon Montaner, Claude Le Men, Johanne Teychené, Christine Lafforgue, Nicolas Dietrich, Chung-Hak Lee, Christelle Guigui

Article

EXPERIMENTAL SOLID-LIQUID MASS TRANSFER AROUND FREE-MOVING PARTICLES IN AN AIR-LIFT MEMBRANE BIOREACTOR WITH OPTICAL TECHNIQUES

Naila Bouayed[1], Manon Montaner[1], Claude Le Men[1], Johanne Teychene[1], Christine Lafforgue[1], Nicolas Dietrich[1,*], Chung-Hak Lee[2] and Christelle Guigui[1]

[1] Toulouse Biotechnology Institute (TBI), Université de Toulouse, CNRS, INRAE, INSA, Toulouse, France
[2] School of Chemical and Biological Engineering, Seoul National University, Seoul 151-744, Republic of Korea
* Correspondence: nicolas.dietrich@insa-toulouse.fr

Abstract: This article focuses on the study of the mass transfer involved in the application of a bacterial antifouling technique for Membrane Bioreactors (MBR) via the addition of solid media. These alginate objects can contain a biological system capable of producing an enzyme degrading the signal molecules responsible for membrane fouling. The objective of this article is to quantify the mass transfer by distinguishing two main types: the transfer from liquid to the "solid media" and the transfer from "solid media" to the liquid phase. For this purpose, a model molecule was chosen, and experiments were specifically developed with an optical device to track the concentration of the dye in the liquid phase, considering three different shapes for the particles (beads, hollow cylinders and flat sheets). The experiments were first performed in jar tests and then in a lab-scale reactor. Results revealed that the total amount of dye transferred into the sheets was greater than that transferred into the cylinders or the beads, which was attributed to the sheets having a larger exchange area for the same volume. When the dyed media were implemented in the MBR (loading rate of solid media 0.45 % v/v – no biomass), the global transfer coefficient from the sheets to the liquid was found to be greater than for the other shapes, indicating a faster transfer phenomenon. The effect of aeration in the MBR was investigated and an optimal air flowrate to foster the transfer was found, based on the highest transfer coefficient that was obtained. This study provides key information about mass transfer in MBRs and how it is affected by the particle shapes and the MBR operating conditions.

Keywords: Membrane Bioreactors (MBRs); Air-Lift Reactors (ALRs); Mass Transfer

Citation: Lastname, F.; Lastname, F.; Lastname, F. Title. *Fluids* **2022**, *7*, x. https://doi.org/10.3390/xxxxx

Academic Editor: Firstname Lastname

Received: date
Accepted: date
Published: date

1. Introduction

A membrane bioreactor (MBR) is a wastewater treatment that combines a membrane process (microfiltration, ultrafiltration, etc.) with a biological treatment. Over the last few decades, MBRs have proved to be highly efficient for advanced wastewater treatment and reuse, and have provided high standards of effluent quality, biomass retention, biomass concentrations, organic removal efficiency, and organic loading rate, together with a low production of sludge and a small environmental footprint [1,2]. Yet the extensive development of MBRs for wastewater treatment is still restricted by

membrane fouling, which results from the formation of a fouling layer on the membrane surface [3](deposition and accumulation of solids, biofilm, pore clogging, adsorption of products, etc.). Membrane fouling gives rise to an overall reduction in performance by causing a loss of permeability, thus increasing the energy consumption and the operating costs. Several cleaning methods (physical, chemical and biological) have been developed in attempts to mitigate this phenomenon. One of the most commonly applied is air-sparging, which consists in the injection of bubbles to induce shear stress between two flat membranes, creating an Air-Lift Reactor (ALR) [4–8]. The addition of solid particles, such as synthetic micro-particles , granular activated carbon [9], or other granular scouring agents (reviewed by [10]) has also demonstrated an effective reduction of fouling in MBRs due to a mechanical washing effect. Recently, a novel biological method has been developed for fouling mitigation, related to the perturbation of cell-to-cell communication between bacteria [11–15]. The technique, named "Quorum Quenching", QQ [16] is based on an enzymatic degradation of the signal molecules (AHLs), that are produced for bacterial communication (Quorum Sensing [17], by excreted or intracellular enzymes produced by specific QQ bacteria. Recent works have shown that, when QQ bacteria are immobilized in small capsules and implemented in MBRs, the biofouling phenomenon is considerably inhibited [18]. For more information on the QQ mechanism and its application to MBRs, the reader is invited to consult the reviews by [19–22]. With the development of QQ entrapping methods [21], the mass transfer appeared as one question that it was essential to address, for two main reasons: firstly, as in every (bio)chemical reaction, the mass transfer of the reagents is a key phenomenon as it can be a limiting step. Secondly, the importance of studying the mass transfer involved in QQ is also linked to the different entrapping methods [22–24] that have been developed (introduction of solid beads, hollow cylinders or sheets into the reactors [25] and to the existing kinds of QQ bacteria producing endo-enzyme- or exo-enzyme [25–28]. From these specificities, two cases of mass transfer can be distinguished: from the mixed liquor towards the inner part of solid media, in the case of endo-enzyme degradation, and from the solid media to the mixed liquor in the case of exo-enzyme-mediated QQ. Even though some attempts have been reported in the literature previously cited, the mass transfer phenomena involved in QQ are not fully understood yet and the present study aims to improve this situation. These studies mostly focused on the observation of diffusion (with no liquid flow) at the scale of one single QQ medium.

The experimental approach described here was based on the use of a dye as model molecule in order to quantify the mass transfer at the reactor scale (not only at the QQ media scale). More specifically, the objective was to provide a quantitative characterization of the mass transfer of the molecules involved in QQ, from the liquid to the QQ media and vice versa for different MBR operating parameters (aeration flow rate, kind of QQ media…). In this context, this article offers the determination of mass transfer parameters such as the transferred flux, the mass transfer coefficient, and the Sherwood number [29–31]. On the basis of these quantitative parameters, the effect of the operating conditions on the mass transfer phenomena will be discussed with reference to the effect of the shape of QQ media and will provide valuable suggestions for future research in this area.

2. Materials and Methods

2.1. Physical properties of QQ media

The QQ media used in this study were made of sodium alginate. Three different shapes of media were used in this study: QQ beads, QQ hollow cylinders and QQ sheets (Figure 1).

The physical properties of the QQ media are summarized in Table 1.

Figure 1. Photographs of media used in the study: (a) beads, (b) hollow cylinders, and (c) sheets.

Table 1. Properties of the solid media.

Solid medium	Beads	Hollow cylinders	Sheets
Dimensions (mm)	Diameter: 3.5	Inner diameter: 1.7 Outer diameter: 3.5 Length: 27	Length: 20 Width: 10 Thickness: 0.5
Volume of a particle (mm^3)	22.5	198.5	100
Surface area of a particle (mm^2)	8.5	455.8	400

2.2. Mass transfer experiments

The mass transfer of real signal molecules (such N-acyl-l-homoserine lactones, acyl-HSLs or AHLs) was initially considered in this study. However depending on the considered bacteria, these molecules can have various composition and the analysis of the transfer would require the detection and the quantification of several AHLs. Among the proposed methods, a biological one relying on the use of the reporter strain *A.tumefaciens* is often proposed to detect the AHLs [32,33]. However this method requires perfectly sterile conditions to be maintained, which could not be achieved at the reactor scale. In addition, the amount of AHLs in the mixed liquor is very small, given that these signal molecules are usually produced at very low concentrations (in the range of picograms to nanograms per liter) and that they are

present as a complex mixture with different compounds, an extraction procedure is necessary before their quantification. Several methods to measure the AHL concentration after their extraction have been reported to date and are summarized by [19]. After extraction, AHL's detection by mass-spectrometry (HPLC-MS, GC-MS, LC-MS-MS, UPLC6FTIR-MS, CZE-MS), NMR or IR can be performed. However, the choice was made to study mass transfer at the global scale, rather than at the media scale. Thus, the selection of a mimic molecule (tracer) was preferred. Rose Bengal Lactone is light red to pink powder used as a dye, the main properties of which are presented in Table 2. Like the AHLs, Rose Bengal Lactone contains a lactone group, reason why it was chosen as a model molecule to study the mass transfer.

Table 2. Physicochemical properties of Rose Bengal Lactone.

Chemical formula/Molecular structure	$C_{20}H_4Cl_4I_4O_5$ 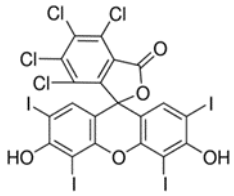
Molecular weight (g.mol^{-1})	973.67
Appearance	Pink powder
Purity	≥ 95 %

The Rose Bengal Lactone was purchased from Sigma-Aldrich. Solutions at a concentration of 0.4 g.L^{-1} were prepared in tap water. In order to help the dissolution of the powder, the solutions were sonicated 3 to 4 times for 15 min and shaken between two sonication cycles, until a clear dark-pink solution was obtained.

The concentration of the dye was determined using optical methods. The absorbance of dye solutions was measured using a spectrophotometer (Jasco-V630, Germany). The measurements were done at 548 nm, wavelength corresponding to the maximum of absorbance in the visible range.

2.2.1. Mass transfer from the liquid to the media

The study of the mass transfer from the liquid phase into the solid medium was performed in jar-tests in order to control hydrodynamic conditions in the different 1L-beaker reactors (Floculateur, Bioblock Scientific). QQ media in a solution of Rose Bengal Lactone (around 0.4 g.L^{-1}) at a solid:liquid volume ratio of 1:9 and under stirring (90 rpm) at room temperature. Two controls without QQ media (one with water and one with the saturated solution of Rose Bengal Lactone) were done to ensure that the observed decrease of concentration in the liquid phase could only be attributed to a transfer into the QQ media, and not to additional phenomena such as natural degradation, precipitation, etc. Liquid samples were collected from the jars every 30 min at first and then spaced out after the first 7 hours. The experiments lasted 24 h, time for the concentration to reach a constant value, corresponding to the stabilization of the system. After 24 h, the stained QQ media were collected and drained to be used for the subsequent experiments.

2.2.2. Mass transfer from the media to the liquid

The mass transfer from the media to the liquid phase was studied in the lab-scale Air-Lift-Membrane-Bio-Reactor (ALMBR) previously described. The QQ media saturated (stained) collected at the end of the jar-test experiments were introduced in a volume fraction of 0.45 % v/v with respected to the total volume of reactor (13 L). The air-lift was set to a riser width of 15 mm. Different operating conditions were investigated in order to highlight the effect of the QQ media shape, as well as the effect of the hydrodynamics (three air flowrates) on the transfer from the QQ media to the liquid phase. Three air flowrates were injected at the bottom of the reactor, corresponding to SAD (Specific Aeration Demand) of 0.75, 0.9 and 1 $Nm^3.h^{-1}.m^{-2}$. In order to visualize the transfer phenomena in the reactor, a camera technique was developed to measure the absorbance (and thus the concentration of Rose Bengal Lactone in the liquid phase) and consisted in using a 12-bit (4096 gray level) CMOS camera (Basler-Ace Aca1920-155 um) equipped with a green filter (495 to 505 nm). A backlight panel (Phlox-LedW-BL, 400 x 200 mm^2, 24 V, 2A, Phlox) was set behind the reactor as presented in Figure 2. The observation window was 97.5 mm wide and 150 mm long and was located at the bottom of the reactor (under the membrane) so that the whole depth of the tank could be observed (thanks to the clear baffles). The camera technique was preferred to a simple absorbance measurement via a light sensor because of the coexistence of three phases in the reactor: gas, liquid and solid, which can be taken into account more accurately thanks to image processing.

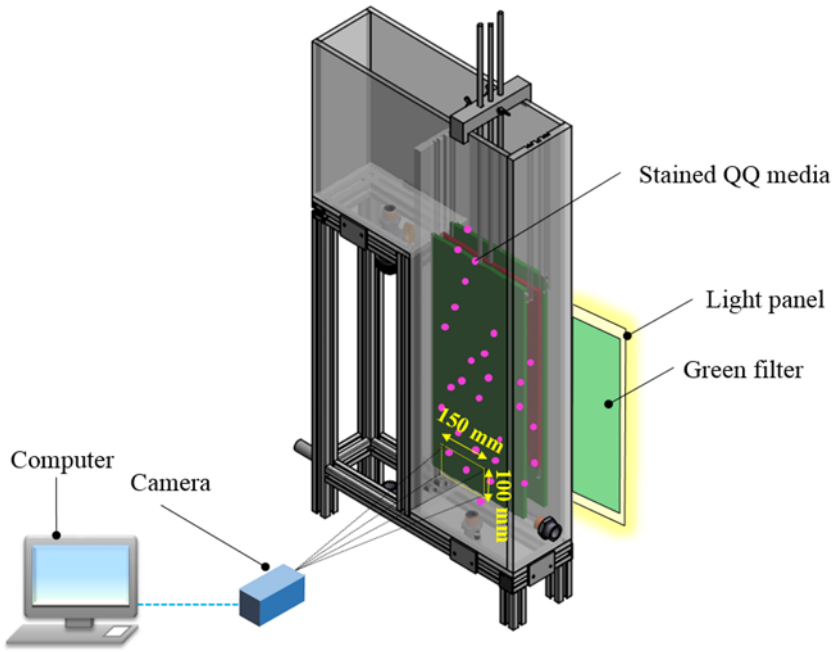

Figure 2. Experimental setup for the visualization of the mass transfer in the MBR.

An image was recorded every 10 s (acquisition frequency of 0.1 Hz) and the total acquisition time was 1 day or more, depending on the time required to reach equilibrium. The size of the images was 1000 x 650 pixels ² (1 pixel = 150 µm). Pylon software (Basler, Germany) was used to control the camera and to configure all of its settings.

The filter was used to narrow down the range of wavelengths passing through the liquid in the reactor to approach a monochromatic beam (~ 500 nm, for which the absorbance is high enough for measurement accuracy) and to link the intensity of light to the concentration of Rose Bengal Lactone, according to the Beer-Lambert law (Equation 1), where A is the instantaneous absorbance, I is the instantaneous light intensity, I_o is the light intensity through the blank (water), C is the concentration of Rose Bengal Lactone, l is the optical path length and ε_λ is the molar attenuation coefficient. The latter coefficient was obtained from the calibration.

$$A = -log\left(\frac{I}{I_0}\right) = \varepsilon_\lambda . l . C \quad (1)$$

Images of standard solutions of Rose Bengal Lactone with known concentrations (Table 2) were recorded using the camera setup and the absorbance of these solutions was also measured using the spectrophotometer at 500 nm (Table 3).

Table 3. Spectrophotometer and camera-deduced optical parameters for standard solutions of Rose Bengal Lactone.

Concentration of dye Lactone solution C (g.L^{-1})	**0.0002**	**0.0006**	**0.0012**	**0.0023**	**0.0044**
Spectrophotometer					
Absorbance at 500 nm $A_{spectro}$ (-)	0.0037	0.0088	0.0188	0.0346	0.0673
Optical path length $l_{spectro}$ (cm)			1.0		
$\frac{A_{spectro}}{l_{spectro}}$ (cm^{-1})	0.0037	0.0088	0.0188	0.0346	0.0673
$\varepsilon_{500\,nm}$ (L.g^{-1}.cm^{-1})			15.136		
Camera					
Absorbance at 500 nm A_{camera} (-)	0.0490	0.1000	0.2050	0.4180	0.7960
Optical path length l_{camera} (cm)			11.6		
$\frac{A_{camera}}{l_{camera}}$ (cm^{-1})	0.0042	0.0086	0.0177	0.0360	0.0686
$\varepsilon_{500\,nm}$ (L.g^{-1}.cm^{-1})			15.425		

The absorbances per unit of optical path length are plotted on the same graph for comparison in Figure 3. It can be observed that the ratios of the absorbance to the optical path length are very close for both measurement techniques. Also, the attenuation coefficients $\varepsilon_{500\,nm}$ were found to be very close (Table 2), with less than 2 % deviation. From this comparison, it is possible to conclude that the camera technique that was specifically developed for the study of the mass transfer in the ALMBR, indeed allowed the measurement of an absorbance which followed the Beer-Lambert law. Given these results, the camera was selected as the only measurement technique to study the dye transfer from the QQ media to the liquid phase in the ALMBR.

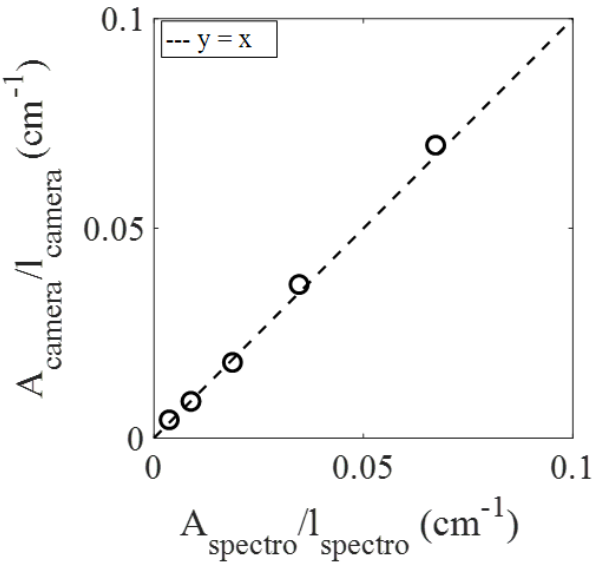

Figure 3. Comparison of the ratios of the absorbance to the optical path length obtained by the spectrophotometer and the camera technique.

The images recorded during the experiments were processed using a Matlab (MathWorks, USA) program. Prior to each experiment (before the addition of the stained solid medium), around 60 images of the blank (tap water) in the reactor were recorded to determine the intensity I_o, and 100 images were recorded of the dark (turning the light panel off) for further calibration of the sensitivity of the measurement. After defining the total number of images to be processed, the acquisition period was selected and a threshold factor of 60 % (used to remove the bubbles or solid media from the image) was applied.

The matrices corresponding to the dark images were first averaged. This average dark image was subtracted from the images to be processed in order to attenuate the signal noise (especially at low intensities). The resulting matrices of the blank gave "flat" matrices that were averaged in a single flat matrix. In the same way, the raw images of the experiment were processed by subtracting the matrix of the average dark image. In the following step, the threshold factor was applied in order to remove the objects (bubbles and solid particles) and only keep the pixels corresponding to the liquid phase (intensity > 60 % of maximum intensity). The mean intensity I of the processed image was then determined by averaging the remaining pixels and the intensity I_0 was obtained by averaging the intensities of the corresponding pixels (in the same location) on the flat matrix. Finally, the corresponding absorbance A was determined according to Equation 1.

First of all, the stability of the Rose Bengal Lactone over time was evaluated by introducing a solution of known concentration into the reactor and using the camera to measure the light intensity of the light panel through this solution over time. The dye was found to be sensitive to strong, long-term exposure to the light panel, as the intensity recorded increased (concentration decrease) over time. Thus, the strength of the light panel was adjusted with a view to avoiding the degradation of Rose Bengal Lactone during the experiment so as to be able to draw reliable conclusions on the mass transfer.

3. Liquid-solid mass transfer from the liquid to the solid medium

3.1. Analysis of the adsorption kinetics

The main mathematical models proposed in the literature to describe the overall adsorption phenomenon are based on the quantity $q(t)$ of solute adsorbed per unit mass of solid (in mg.g^{-1}). The pseudo-first-order model was proposed by Lagergren in 1898 [34] and is expressed according to Equation 1, where q_e is the adsorbed quantity reached per unit of mass at equilibrium, and k_1 is the constant of the pseudo-first-order kinetics (in s^{-1}). Determining this constant requires the linearization of Equation 2, which results in Equation 3, where k_1 is the slope of the curve $\ln(q_e - q(t))$ versus time.

$$\frac{dq(t)}{dt} = k_1\left(q_e - q(t)\right) \quad (2)$$

$$\ln(q_e - q(t)) = ln(q_e) - k_1 t \quad (3)$$

Another model, the pseudo-second-order model [35] , assumes the existence of strong chemical bonds between the solute molecule and the solid. This model is described by Equation 4, where k_2 is the constant of the pseudo-second-order kinetics (in g.mg^{-1}.s^{-1}). The linear form presented in Equation 5 allows the constant k_2 as well as the adsorbed quantity at equilibrium, q_e to be determined.

$$\frac{dq(t)}{dt} = k_2\left(q_e - q(t)\right)^2 \quad (4)$$

$$\frac{t}{q(t)} = \frac{t}{q_e} + \frac{1}{k_2 q_e^2} \quad (5)$$

In the present case, the adsorbed quantity at time t, $q(t)$, can be deduced from Equation 6, where Ms is the mass of solid particles, ρ_s and V_s are the wet density (in kg.m^{-3}) and the total volume (in m^3), respectively, of the solid particles, $C_l(t)$ is the concentration in the bulk, and V_l is the total liquid volume.

$$q(t) = \frac{C_l(t=0) - C_l(t)}{M_s} V_l = \frac{C_l(t=0) - C_l(t)}{\rho_s V_s} V_l \quad (6)$$

The jar-test experiments were repeated three times. The results are presented in Figure 4, in terms of the total amount of Rose Bengal Lactone per unit of mass of medium ($q(t)$) (defined in Equation 6) for the different shape of QQ media.

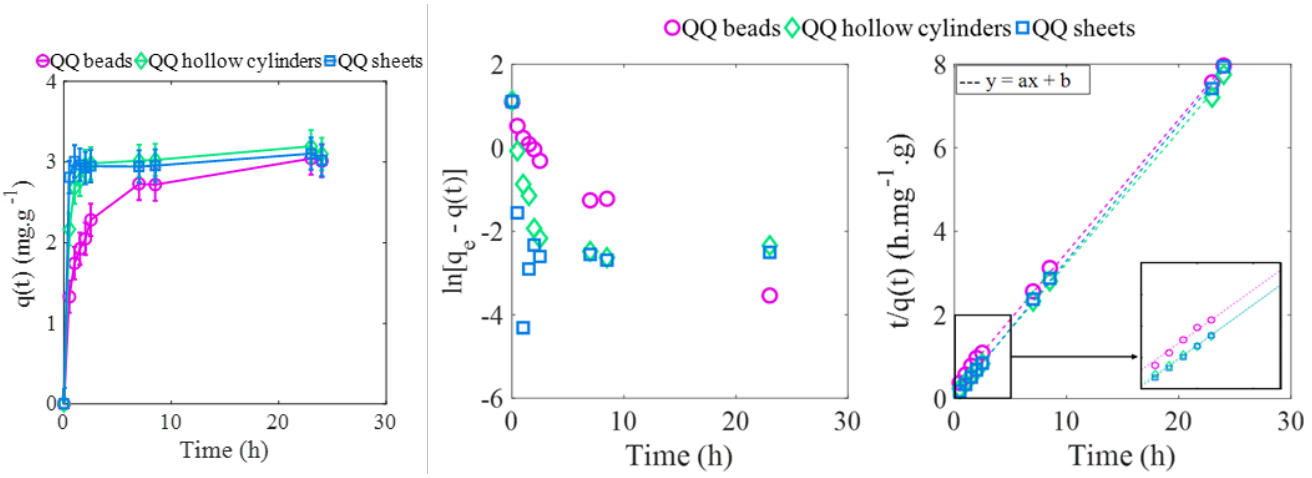

Figure 4. (Left) Amount of Rose Bengal Lactone transferred in the solid media over time. (Middle) and (Right) Identification of the adsorption model parameters for the experimental data. Jar-test experiments.

The curves in Figure 4 describe a very rapid increase in the first hour and then an overall slowdown until equilibrium is reached after 24 h. This kind of trend is typical of a mass transfer phenomenon in which the gradient of concentrations tends to decrease over time, thus slowing down the increase of the total amount transferred. A comparison of the three experiments performed for each media reveals that the jar-test experiment was repeatable, with less than 10 % standard deviation between the three final values of the amount of Rose Bengal Lactone transferred and a similar time evolution for the experiments done with a same QQ medium.

The comparison of the three curves obtained for three media shapes in Figure 5 suggests that the global adsorption dynamics depends on the shapes of QQ media. In addition, the time to reach 96 % of the final value was 0.5 h and 2 h for sheets and hollow cylinders, respectively, whereas, for beads, this time was much longer - about 8.5 h. According to the adsorption theory previously presented, the pseudo-first- and pseudo-second-order models were considered to describe the kinetics of the phenomenon under study. The variations of $ln[q_e - q(t)]$ and $\frac{t}{Q}$ over time were thus deduced from the experimental data and are presented in Figure 4. The variations of $ln[q_e - q(t)]$ over time do not show a linear trend, unlike the variations of $\frac{t}{Q}$, which suggests that the pseudo-second-order model could be more appropriate ($R^2 > 0.99$) to describe the adsorption phenomenon. The parameters of the linear correlations ($y = ax + b$) are presented in Table 4. The parameters of the pseudo-second order adsorption model (k_2 and q_e) are deduced from the linear correlation parameters a and b (from Equation 5), according to Equations (7) and (8).

$$q_e(calculated) = \frac{1}{a} \quad (7)$$

$$k_2 = \frac{a^2}{b} \quad (8)$$

Table 4. Linear correlation and parameters of the pseudo-second-order kinetics model for the adsorption of Rose Bengal Lactone onto solid media. Jar-test experiments.

	beads	hollow cylinders	sheets
Linear correlation parameters ($y = ax + b$)			
a (g.mg^{-1})	0.3187	0.3157	0.3260
b (h.mg^{-1}.g)	0.3015	0.0712	0.0376
R^2	0.9996	0.9995	0.9996
Model parameters			
q_e (calculated) (mg.g^{-1})	3.14	3.17	3.07
q_e (experimental)	3.0 ± 0.2	3.1 ± 0.2	3.0 ± 0.2
k_2 (g.mg^{-1}.h^{-1})	0.34	1.40	2.83
k_2 (10^{-5} g.mg^{-1}.s^{-1})	9.36	38.89	78.51
$k_2 q_e$ (10^{-4} s^{-1})	2.94	12.33	24.10

It appears first that the calculated maximal amounts q_e of Rose Bengal Lactone adsorbed at equilibrium (also representing the adsorption capacities of the media), are very close to the experimental values reached after 24 h (Figure 4), with discrepancies of less than 5 %, which confirms that the phenomenon studied has reached the stable state after 24 h, even for the beads. When comparing the final amounts, q_e, reached for the three shapes in each experiment, the differences were not significant, since the three (experimental) values differ by less than 5 %. This finding indicates that the shape of the solid media has no effect on their adsorption capacities, which is consistent since the media are made from the same material. However, significant differences appear in the pseudo-second-order rate constant of adsorption k_2 (representing the adsorbed flux per unit of mass of solid media), since it was found to be, respectively, 12 and 24 times greater for the hollow cylinders and sheets, than for the beads (Table 4). This trend is confirmed by observation of the adsorption rate index ($q_e k_2$) defined by [35], which purely reflects the kinetic performance of the system. Thus, considering the same volumes of solid media, the adsorption kinetics performance for sheets is considerably greater than for the hollow cylinders and beads.

Knowing that the adsorption phenomenon involves a succession of mechanisms (external mass transfer, internal mass transfer, pore diffusion, etc.), and that the constant k_2 englobes all of these mechanisms, these results prove that the differences between the three shapes of solid particles necessarily originate in at least one of the steps.

3.2. Analysis of the external liquid-solid mass transfer mechanism

According to the method proposed by Furusawa and Smith [36], the external mass transfer step is related to the changes of concentrations over time by the mass balance expressed in Equation 9, where k_{ls} is the liquid-solid mass transfer coefficient (in m.s^{-1}), S_s is the total area of the liquid-solid interface (in m^2) , V_l is the total liquid volume, $C_l(t)$ and $C_s(t)$ are the concentration in the bulk and the concentration at the surface of the solid particles respectively. A simple method was proposed to deduce k_{ls}, and consists

in substituting Equation 9 with the corresponding values at the initial conditions (when $t \to 0$), which results in Equation 10. Therefore, the liquid-solid external mass transfer coefficient k_{ls} can be deduced from the initial slope [$(\frac{dC_l(t)}{dt})_{t=0}$] of the curve $C_l(t)$ versus time. This approach has been adopted in the literature to study different systems involving liquid-solid mass transfer, some examples of which are the removal of food dyes using chitosan particles [37,38] or the transfer of ions using ion-exchange resin [39].

$$\frac{V_l dC_l(t)}{dt} = -k_{ls}S_s\left(C_l(t) - C_s(t)\right) \quad (9)$$

$$(\frac{dC_l(t)}{dt})_{t=0} = \frac{-k_{ls}S_s}{V_l}C_l(t=0) \quad (10)$$

This approach is based on the assumption that the concentration in the liquid, $C_l(t)$, is uniform. The evolution of the concentration in the liquid phase $C_l(t)$, is presented in Figure 5.

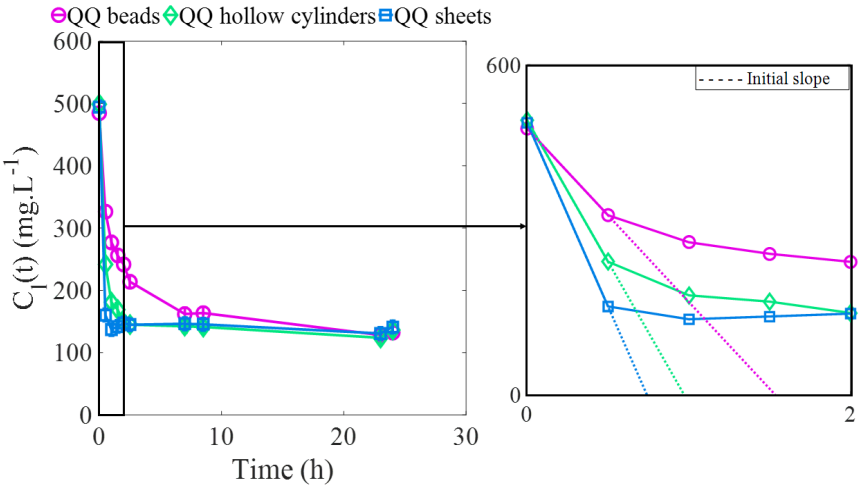

Figure 5. Concentration of the Rose Bengal Lactone in the liquid phase over time. Jar-test experiments.

In order to evaluate the external mass transfer coefficient, the initial slope $(\frac{dC_l(t)}{dt})_{t=0}$ of each curve was determined (Figure 5) and used to calculate the external mass transfer k_{ls} via Equation 10, which resulted in Equation 11. The results are presented in Table 5.

$$k_{ls} = -\frac{V_l}{S_s C_l(t_0)}(\frac{dC_l(t)}{dt})_{t=0} \quad (11)$$

Table 5. External liquid-solid mass transfer parameters for the three media shapes and the three experiments repeated for each shape. Jar-test experiments (under 90 rpm and solid:liquid ratio of 1:9).

	beads	**hollow cylinders**	**sheets**
Experiment 1			
$\boldsymbol{Ss}$ (m^2)	0.100	0.135	0.234
$\boldsymbol{Cl(t=0)}$ ($mg.L^{-1}$)	484	499	495
$(dC_l(t)dt)_{t=0}$ ($mg.L^{-1}.h^{-1}$)	- 316	- 514	- 668
$\boldsymbol{k_{ls}S_s}$ ($10^{-7}\ m^3.s^{-1}$)	0.95	1.51	1.98
$\boldsymbol{k_{ls}}$ ($10^{-6}\ m.s^{-1}$)	0.95	1.12	0.85
Experiment 2			
$\boldsymbol{Ss}$ (m^2)	0.086	0.115	0.200
$\boldsymbol{Cl(t=0)}$ ($mg.L^{-1}$)	424	409	436
$(dC_l(t)dt)_{t=0}$ ($mg.L^{-1}.h^{-1}$)	- 320	- 455	- 612
$\boldsymbol{k_{ls}S_s}$ ($10^{-7}\ m^3.s^{-1}$)	0.94	1.39	1.75
$\boldsymbol{k_{ls}}$ ($10^{-6}\ m.s^{-1}$)	1.12	1.21	0.88
Experiment 3			
$\boldsymbol{Ss}$ (m^2)	0.086	0.115	0.200
$\boldsymbol{Cl(t=0)}$ ($mg.L^{-1}$)	506	492	503
$(dC_l(t)dt)_{t=0}$ ($mg.L^{-1}.h^{-1}$)	- 300	- 456	- 639
$\boldsymbol{k_{ls}S_s}$ ($10^{-7}\ m^3.s^{-1}$)	1.14	1.74	2.38
$\boldsymbol{k_{ls}}$ ($10^{-6}\ m.s^{-1}$)	1.30 ± **0.1**	1.51± **0.2**	1.19 ± **0.1**
Average values over the three experiments ± standard deviation			
$\boldsymbol{k_{ls}S_s}$ **($10^{-7}\ m^3.s^{-1}$)**	**1.0 ± 0.1**	**1.5 ± 0.2**	**2.0 ± 0.2**
$\boldsymbol{k_{ls}}$ **($10^{-6}\ m.s^{-1}$)**	**1.1 ± 0.2**	**1.3 ± 0.2**	**1.0 ± 0.2**
$\boldsymbol{L}$ **(10^{-3} m)**	1.75	0.45	0.25
$\boldsymbol{D}$ **($10^{-10}\ m^2.s^{-1}$)**		3.92	
$\boldsymbol{Sh}$	**4.9 ± 0.4**	**1.5 ± 0.1**	**0.6 ± 0.08**

The product $k_{ls}S_s$, representing the transferred flux, describes the same trend as the adsorption kinetics parameters (greater for sheets than for hollow cylinders and beads). Despite the uncertainty in the product $k_{ls}S_s$, for the different QQ shapes that can reach 30 %, the differences between the three shapes are significant (on average 50 % between beads and cylinders, and 33 % between cylinders and sheets). This result confirms the assumptions made in the adsorption analysis that the shapes of media induce significant differences in the external mass transfer step of the whole phenomenon. In particular, the external mass transfer is governed by the external surface area of the solid medium, which explains the greater flux obtained for the sheets. It should be pointed out that in the case of cylinder, the considered surface is the total one (sum of external, internal and sides surfaces) and it is obvious that the liquid renewal inside the cylinder can be weak. Therefore, the measurement of the global transfer at the begining of the experiement could be affected by a concentration of dye inside the QQ media lower than that measured in the liquid bulk. The external mass transfer coefficient k_{ls} was determined for the three shapes (Table 5). On average, an 18 % difference was found between the mass transfer coefficients of the beads and the hollow

cylinders, and a 30 % difference between hollow cylinders and sheets, which can be viewed as insignificant (< 30 %). Therefore, the external mass transfer coefficient for the three shapes of media can be considered as similar, which is consistent with the fact that the hydrodynamic conditions created in the jar-tests were similar. Knowing the external liquid-solid mass transfer coefficient as well as the diffusion coefficient of Rose Bengal in water, the Sherwood number could be determined for each condition according to Equation 12.

$$Sh = \frac{k_{LS}L}{D} \quad (12)$$

In order to take account of the fact that the transfer occurs from all around a solid particle to its center, the characteristic length L in Equation 12 was taken to be the radius for the beads, and half the thickness for both the hollow cylinders and the sheets. According to the literature [38] , the external convective mass transfer step is completely prevalent for Sh < 0.5, whereas the diffusion is significant for Sh > 10. In the present case (Table 5), the Sherwood numbers roughly ranged between 0.5 and 5, and thus were between 0.5 and 10, indicating that there was no strong predominance of one mechanism over another under the conditions investigated. This result shows that the internal diffusion and the external convection can be considered as two mechanisms of equivalent importance, both governing the overall transport of molecules from the bulk to the solid media. In addition, when the three shapes of solid media particles were compared, the greatest Sherwood number was obtained for the solid beads, which means that the internal diffusion in this shape is more significant than for the other two shapes.

To conclude, with the perspective of applying quorum quenching for biofouling mitigation by using endo-enzyme-producing bacteria (such as *Rhodococcus* sp. BH4), the (external) mass transfer of AHLs from the mixed liquor towards the core of the media could be favored, in terms of transferred flux ($k_{ls}S_s$), by the presence of sheets rather than the other two shapes for the same volume of medium. The beads seem to be the least favorable shape for mass transfer: not only does their small surface area give rise to the lowest transferred flux ($k_{ls}S_s$) (in comparison to the other shapes) but their great diameter also slows down the internal transfer step. Considering that quorum quenching is based on an enzymatic reaction, further investigation is needed to know whether the transferred flux or the transfer kinetics of AHLs (substrate) towards enzymes is the key parameter to promote when the aim is to reduce biofilm formation effectively.

4. Solid-liquid mass transfer from the solid media to the liquid

In the case of the experiments conducted in the aerated lab-scale ALMBR, the transfer of the Rose Bengal Lactone took place from the solid media to the liquid. Different operating conditions were investigated to highlight the effect of the solid medium shape (beads, hollow cylinders and flat sheets), as well as the effect of the hydrodynamics (three air flowrates, Specific Aeration Demand, called SAD, of 0.75, 0.9 and 1 $Nm^3.h^{-1}.m^{-2}$) on the transfer from the solid media to the liquid phase. This kind of configuration (solid-liquid) has been much less investigated than the previous one (liquid-solid), especially under similar hydrodynamic conditions. Although it can be assumed that transfer from the solid to the liquid is a combination of several mechanisms, as illustrated in Figure 6, to the best of our knowledge, no complete model of the whole phenomenon, taking all the steps involved into account, is reported in the literature.

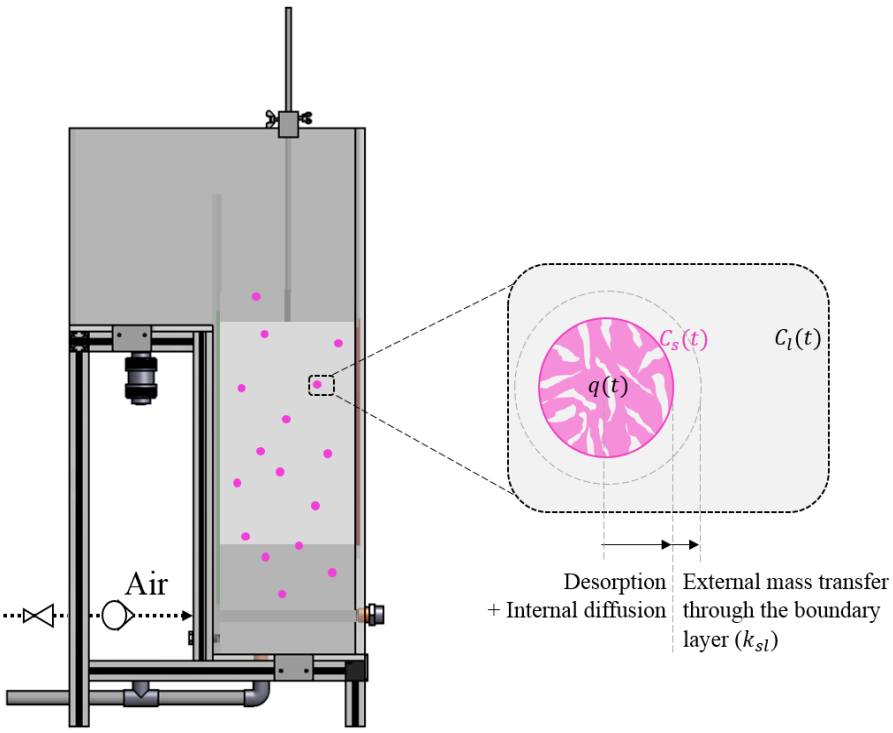

Figure 6. Illustrative representation of the transfer of Rose Bengal Lactone from the solid medium to the liquid, in the aerobic tank of the lab-scale MBR.

Some studies have focused on characterizing the solid-liquid mass transfer involved in the dissolution of solid substances in their own solution, using the mass balance presented in Equation 13 [40]. This approach, similarly, to the one developed for the liquid-solid mass transfer (the opposite phenomenon) (Equation 9), allows a coefficient k_{sl} to be determined for the solid-liquid external mass transfer. The solid-liquid mass transfer coefficient can be deduced from Equation 14, which corresponds to the very early stage of the operation (when $t \to 0$) at which the concentration in the liquid is equal to zero and the initial concentration at the surface of the solid $C_s(t=0)$ can be considered as homogeneous in the solid media, and equals the ratio of the initial mass of dye (m_0) adsorbed on the QQ media to the total volume of solid media V_s. In practice, k_{sl} is deduced from the initial slope of the curve $C_l(t)$ versus time.

$$\frac{V_l dC_l(t)}{dt} = k_{sl}S_s\left(C_s(t) - C_l(t)\right) \quad (13)$$

$$\left(\frac{dC_l(t)}{dt}\right)_{t=0} = \frac{k_{sl}S_s}{V_l}C_s(t=0) = \frac{k_{sl}S_s m_0}{V_l V_s} \quad (14)$$

Mass transfer from the media to the liquid phase was studied in the ALMBR under different aeration conditions in order to evaluate how the hydrodynamics and the QQ media shape could influence the transfer. However, before analyzing the results, it is worth mentioning that, in the case of this study, it can be assumed that the hydrodynamics is involved at several levels in the mass transfer phenomenon: by promoting turbulence in the liquid phase, it can reduce the concentration gradient between the surface of the media and the bulk and, thus, accelerate the mass transfer phenomenon; at

the local scale, it can enhance the motion of the particles, and therefore favor the fast renewal of the liquid boundary layer around them; in addition air flowrate affects the proportion of fluidized QQ media in the reactor, and thus control the exchange surface between the solid media and the liquid phase. Therefore, it can be assumed that the effect of hydrodynamics on the global mass transfer is complex because of the coupling of all these phenomena. For each air flowrate, the total surface corresponding to the added QQ media S, the surface corresponding to the moving particles (fluidized ones) S_{FM} , and the volume of these suspended QQ media V_{FM} are reported in Table 6. Since the used QQ media are those obtained at the end of the Jar tests, their initial dye concentration is known.

Table 6. Solid media properties in the ALMBR under different air flowrates.

SADm ($Nm^3.h^{-1}.m^{-2}$)	**0.75**			**0.90**			**1.00**		
Solid medium	Beads	Hollow cylinders	Sheets	Beads	Hollow cylinders	Sheets	Beads	Hollow cylinders	Sheets
Tot. exchange surf. area S_s (m^2)	0.086	0.115	0.200	0.086	0.115	0.200	0.086	0.135	0.234
Fluidization rate (%)	6.2	26.2	30.1	10.9	53.2	47.8	16.1	63.3	55.9
Fluidized surface area S_{FM} (m^2)	0.0062	0.0354	0.0704	0.0109	0.0718	0.1118	0.0161	0.0845	0.1308
Fluidized volume V_{FM} (10^{-5} m^3)	0.31	1.53	1.76	0.64	3.11	2.79	0.94	3.70	3.27

4.1. Effect of hydrodynamics on solid-liquid mass transfer

Using the camera and the image processing, the concentration of Rose Bengal Lactone over time was monitored when the stained QQ media were introduced into the ALMBR, under the conditions presented in Table 6. The results are presented in Figure 7, in terms of normalized amount of dye ($\frac{C_l(t)V_l}{m_0}$) released to the liquid overtime. It is first possible to observe that the overall aspect of the curves includes a rapid increase at the beginning and then tends to a stable value. This kind of trend was to be expected since, in this case, the mass transfer is driven by the difference of concentrations between the solid and the liquid, which tends to be attenuated over time, inducing a slowdown of the transfer. The overall mass transfer phenomenon appears to be relatively slow, since all the experiments lasted more than 24 h. The time required to approach the equilibrium (the moment t_e at which the normalized concentration reached 96 % of its final value) was measured for each condition. The times t_e for the three different air flowrates were quite similar for a given shape of solid media. It could then be assumed that the global transfer dynamics was not significantly affected by the aeration in the range of air flowrates investigated.

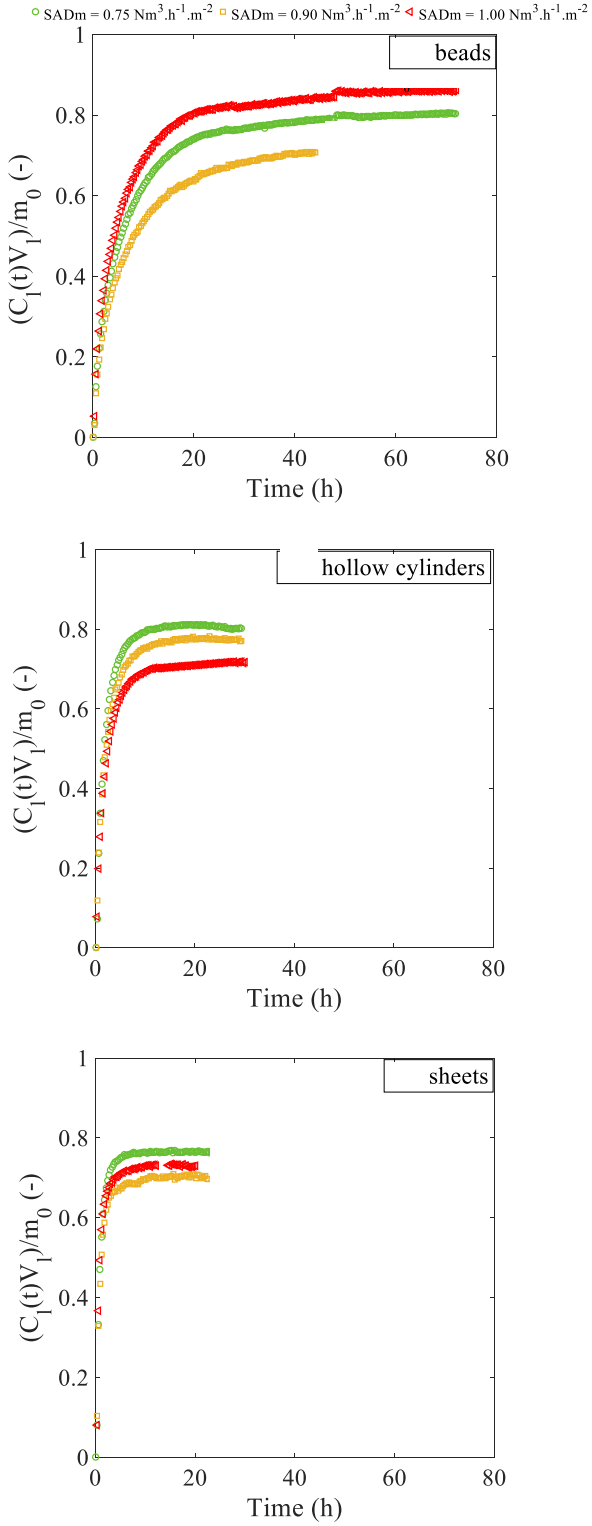

Figure 7. Effect of the hydrodynamics on the normalized amount of Rose Bengal Lactone released into the liquid phase for the three different shapes of solid media. ALMBR experiments.

In addition, the solid-liquid mass transfer pforùatarameters (k_{sl} and $k_{sl}S_{exchange}$, where $S_{exchange}$ is the exchange surface between the solid medium and the liquid phase) were determined considering the initial conditions ($t \to 0$) and according to the approach explained previously (Equations 13 and 14). The initial slopes of the curves $C_l(t)$ were determined over the first 10 points (the first 90 s of the operation) for each condition, and one example is presented in Figure 8 for the mass transfer from the beads to the liquid under the three air flowrates investigated.

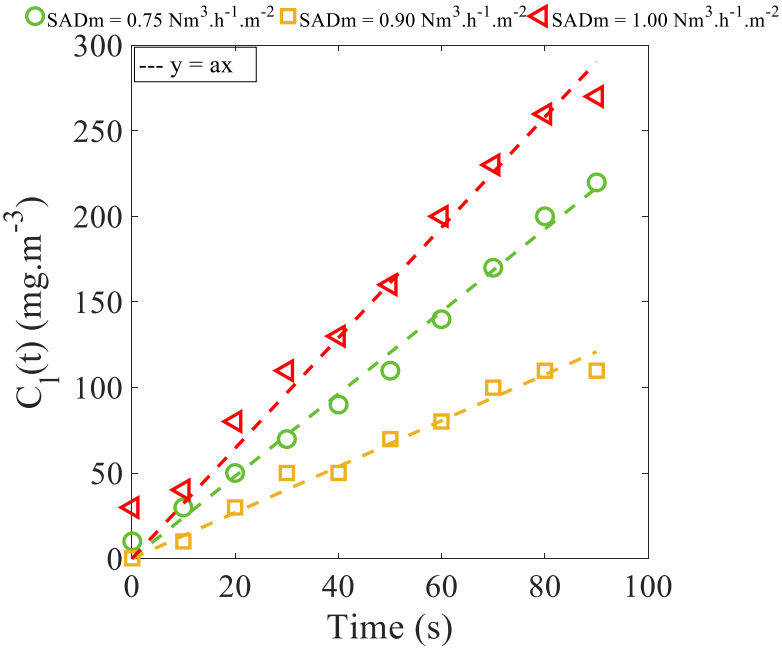

Figure 8. Initial evolution (over the first 90 s) of the concentration of Rose Bengal Lactone in the liquid phase using beads with three air flowrates. ALMBR experiments.

The correlation parameters and the mass transfer parameters are grouped in Table 7 as the mass transfer parameters obtained for the different shapes. The observation of the transferred flux $k_{sl}S_{exchange}$ reveals no clear effect of the aeration, in the range investigated, since different trends are described for the three shapes of solid media. The determination of the mass transfer coefficient k_{sl} requires the transferred flux that was measured to be divided by the exchange surface area $S_{exchange}$ to compare the transfer kinetics. However, in the present case, the exact exchange surface area is hard to evaluate, since it depends on the fluidization of the solid media, as previously mentioned. Therefore, two possible limit-cases could be considered for discussion: in the first case, the exchange surface area corresponds to the total surface S_s of solid medium introduced in the reactor, whether the particles are fluidized or settled. In the second case, the exchange surface corresponds to the surface area S_{FM} of the fluidized particles only. The mass transfer coefficients were calculated in both cases (Table 7) and are also represented as a function of the aeration for the three shapes of solid media in Figure 9.

Table 7. Parameters of the mass model and Sherwood numbers for the solid-liquid mass transfer of Rose Bengal Lactone from the medium to the liquid under different air flowrates (*the Sh numbers were calculated with the diffusion coefficient* $D = 3.92 \times 10^{-10}$ $m^2.s^{-1}$). ALMBR experiments.

SADm ($Nm^3.h^{-1}.m^{-2}$)	**0.75**	**0.90**	**1.00**
Solid-Liquid mass transfer parameters for beads			
Tot. exchange surf. area S_s (m^2)	0.086	0.086	0.086
Fluidization rate (%)	6.2	10.9	16.1
Fluidized surface area S_{FM} (m^2)	0.062	0.0109	0.01611
Fluidized volume V_{FM} (10^{-5} m^3)	0.31	0.64	0.94
$k_{sl}S_{exchange}$ (10^{-8} $m^3.s^{-1}$)	1.00	0.62	1.52
k_{sl} (considering S_s) (10^{-7} $m.s^{-1}$)	1.17 ± **0.1**	0.72± **0.06**	1.78 ± **0.15**
k_{sl} (considering S_{FM}) (10^{-7} $m.s^{-1}$)	18.8± **01**	6.8± **0.5**	11± **1**
L (10^{-3} m)		3.50	
Sh (considering S_s) (-)	1.04	0.66	1.59
Sh (considering S_{FM}) (-)	16.80	6.08	9.86
Solid-Liquid mass transfer parameters for hollow cylinders			
Tot. exchange surf. area S_s (m^2)	0.115	0.115	0.135
Fluidization rate (%)	26.2	53.2	63.3
Fluidized surface area S_{FM} (m^2)	0.0354	0.0718	0.0845
Fluidized volume V_{FM} (10^{-5} m^3)	1.53	3.11	3.70
$k_{sl}S_{exchange}$ (10^{-8} $m^3.s^{-1}$)	2.16	1.70	1.87
k_{sl} (considering S_s) (10^{-7} $m.s^{-1}$)	1.88± **0.1**	1.48± **0.1**	1.39± **0.1**
k_{sl} (considering S_{FM}) (10^{-7} $m.s^{-1}$)	7.16± **0.6**	2.86± **0.3**	2.20± **0.2**
L (10^{-3} m)		0.90	
Sh (considering S_s) (-)	0.43	0.35	0.32
Sh (considering S_{FM}) (-)	1.65	0.66	0.50
Solid-Liquid mass transfer parameters for sheets			
Tot. exchange surf. area S_s (m^2)	0.200	0.200	0.234
Fluidization rate (%)	30.1	47.8	55.9
Fluidized surface area S_{FM} (m^2)	0.0704	0.01118	0.1308
Fluidized volume V_{FM} (10^{-5} m^3)	1.76	2.79	3.27
$k_{sl}S_{exchange}$ (10^{-8} $m^3.s^{-1}$)	4.03	3.23	4.58
k_{sl} (considering S_s) (10^{-7} $m.s^{-1}$)	2.02± **0.2**	1.62± **0.1**	1.95± **0.2**
k_{sl} (considering S_{FM}) (10^{-7} $m.s^{-1}$)	6.63 ± **0.5**	3.37± **0.3**	3.50± **0.3**
L (10^{-3} m)		0.50	
Sh (considering S_s) (-)	0.26	0.21	0.25
Sh (considering S_{FM}) (-)	0.85	0.43	0.45

Significant differences can be observed between the two cases considered. In the first case, where the totality of solid media introduced (with surface area S_s) in the reactor is assumed to participate in the global transfer, the mass transfer coefficients range roughly between 0.5×10^{-7} and 2.0×10^{-7} m.s^{-1}.

In the second case, where the assumption is that only the fluidized particles (with surface area S_{FM}) participate in the global transfer, the mass transfer coefficients range between 0.2×10^{-6} and 2.0×10^{-6} m.s^{-1}. These observations are consistent and actually indicate that, in the second case, where the number of particles transferring (only the fluidized ones) is lower, the mass transfer would have to be much faster to reach the same transferred flux as in the first case. However, the effect of the air flowrate on the mass transfer coefficient is still hardly identifiable in the investigated range, whichever the case considered.

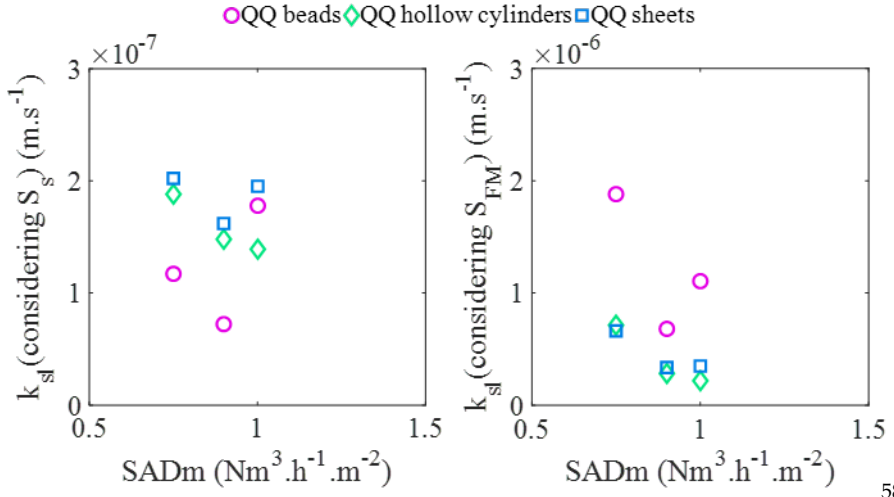

Figure 9. Mass transfer coefficients under different air flowrates and for the three shapes of media particles. ALMBR experiments.

These results show that the effect of the air flowrate on the solid-liquid mass transfer is not clearly identifiable in the conditions investigated, because of the complexity of the mechanisms, which depend on the aeration, and the difficulty of assessing the exchange surface area involved in the transfer with certainty. The two cases considered here are "extreme" cases, which are most likely not representative of the reality since (i) the settled media can also take part in the global transfer and (ii) because there is an alternation phenomenon in the fluidization (the media in suspension are not necessarily the same during the whole operation). Thus, the effective surface area of exchange $S_{exchange}$ between the solid medium and the liquid phase should be somewhere between the surface area of the fluidized particles and the total surface area of the medium ($S_{FM} < S_{exchange} < S_s$).

4.2 Effect of solid particle shapes on the mass transfer

Because the initial conditions were different from one experiment to another and the levels reached at equilibrium were different for the three shapes of solid particles (Figure 7), the concentration curves were normalized with respected to the final value ($\frac{C_l(t)}{C_l(t_\infty)}$) and the curves presented in Figure 10 take only the dynamics of the transfer phenomenon into account (independently of the amounts transferred).

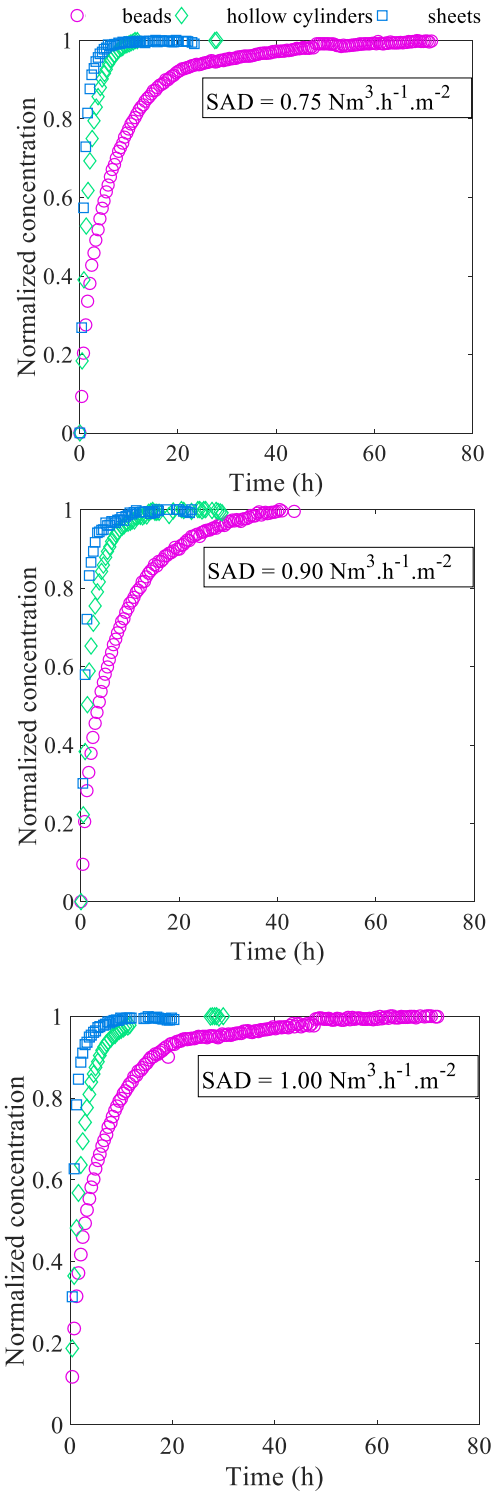

Figure 10. Effect of the shapes of the solid media on the normalized concentrations of Rose Bengal Lactone in the liquid phase for the three different air flowrates. ALMBR experiments.

The effect of the media shapes can be determined first by visualizing the curves, since it appears clearly that the overall dynamics is faster for the sheets than for the hollow cylinders or the beads. This can be confirmed by the comparison of the times t_e necessary to reach 96 % of the equilibrium. It

appears that the time to reach equilibrium for the beads is approximately 3 times greater than that for the hollow cylinders and 9 times that for the sheets, in the range of air flowrates investigated. In the case of beads, the curves presented in Figure 10 reveal that the equilibrium is not completely reached and that the mass transfer continues to evolve very slowly, possibly because of their larger diameter and thus slower internal mass transfer. The mass transfer parameters determined in Table 7 show that significant differences are obtained in the transferred flux $k_{sl}S_{exchange}$ for the three shapes. For example, for a SADm of 1.00 $Nm^3.h^{-1}.m^{-2}$ (corresponding to the highest fluidization rates), $k_{sl}S_{exchange}$ in presence of sheets is up to 3 or 4 times greater than that of beads or hollow cylinders, respectively. In terms of mass transfer coefficient k_{sl} , the differences between the three particle shapes depend on which of the two cases mentioned above is considered. It appears that, for the same volume of solid medim introduced into the reactor, the mass transfer phenomenon is considerably enhanced in the presence of sheets compared to the other shapes, in terms of both time to reach equilibrium and flux transferred. In addition, the time t_e needed to reach equilibrium for sheets is only around 4 h, which represents one third of the residence time (12 h) of the ALMBR, whereas the time needed for beads (about 30 h) is at least 2.5 times greater than the residence time. These results suggest that, among the three shapes of media, sheets would be the most favorable to enhance the mass transfer phenomenon from the medium to the liquid phase, and thus to quickly mitigate fouling via the biological activity. The Sherwood numbers were determined according to Equation 12 for each medium shape and are shown in Table 7. Again, two cases were considered, corresponding to the two exchange surface areas. When the total surface S_s is taken into account, the Sherwood numbers range from 0.2 to 1.6 for the different particle shapes under the different air flowrates. According to the literature, the fact that the Sherwood numbers are lower than 0.5 (in this case for hollow cylinders and sheets) indicates that the diffusion mechanism is very fast compared to the external mass transfer step in the investigated conditions, and that the diffusion time can be considered negligible. However, for the beads ($0.6 < Sh <$ 1.6), the internal diffusion is not negligible, which is consistent with the fact that equilibrium was never completely reached in the investigated conditions. For Sh <1, it has been possible to propose a scaling law between the Sherwood number and the media Reynolds number ($Re = \frac{\rho_{fluid} \times U_{liquid\ in\ the\ riser}\ d_{media}}{\mu_{fluid}}$) with a good precision (22% of standard deviation):

$$Sh = 0.1 \times Re^{0.2} \quad (15)$$

This correlation shows a strong effect of the local hydrodynamics impacted by the particle on the global mass transfer rate of the medium for all the shapes studied. It is worth noting that this correlation could be improved with more data to include other dimensionless number such as the Schmidt number. When the fluidized surface area S_{FM} is considered, the Sherwood numbers are much greater and range from 0.4 to 17. In most cases, the Sherwood numbers are between 0.5 and 10 (except for the beads under 0.75 $Nm^3.h^{-1}.m^{-2}$) which, according to the literature, indicates that there is no clear prevalence of one mechanism over another. However, in the particular case of the beads under a SADm of 0.75 $Nm^3.h^{-1}.m^{-2}$, the Sherwood number is 16.80 (> 10) which refers to a slow diffusion step. In all cases (whatever the exchange surface considered), the Sherwood numbers obtained for the beads

are much higher than for the other two shapes, which undeniably shows that the diffusion into the beads is slower because of their larger diameter.

A comparison of the investigated air flowrates led to the conclusion that no notable effect on the solid-liquid mass transfer coefficient was observed in the conditions of the study. This result could be explained by the fluctuations in the fluidization of media during the experiment and the difficulty of evaluating the effective exchange surface with precision, which made the precise determination of a mass transfer coefficient difficult. Concerning the effect of the media shapes, it was found that the sheets gave rise to greater mass transfer in the shortest time to reach equilibrium and the greatest transferred flux. With a view to applying quorum quenching to reduce membrane biofouling, sheets may therefore be the most appropriate shape in the case of exoenzyme-producing bacteria (*Pseudomonas* sp. 1A1, for example) as the exoenzyme produced in the core of a sheets could rapidly transfer out of it to reach and degrade the AHLs present in the mixed liquor.

Finally, the determination of the Sherwood number in the conditions investigated demonstrated that the overall phenomenon is clearly limited more by the external mass transfer step than by the internal diffusion in the solid media. Nevertheless, comparing the three shapes of media tended to show that the diffusion could again be a little more important in the case of beads, as was the case for the liquid-solid mass transfer, because of their greater diameter.

In order to evaluate the impact of the presence of solid media on a possible membrane clogging, the permeability of the membrane has been measured for several operating conditions. In the case of a constant flow filtration, clogging is characterized by the increase in transmembrane pressure (TMP) over time. A pressure sensor on the permeate side allows to follow the pressure Pp over time. The initial pressure Pi in the reactor is measured at the beginning of the experiment when the pump on the permeate side is stopped. The transmembrane pressure is calculated according to the equation below:

$$\mathrm{TMP}=P_i-Pp \tag{16}$$

The permeability measurement is performed by maintaining a constant volume of water in the reactor. The operation consists of setting the permeate flow rate and following the pressure evolution to determine the permeate flux J and the permeability Lp, and is determined according to the Darcy's law with the following expression:

$$J_{20\,^{\circ}C} = Lp \quad \times TMP = \frac{PTM}{\mu_{20^{\circ}C} \times R_m} \tag{17}$$

Figure 11 represents the evolution of the water permeability at 20 °C as a function of time. It is obtained for a SADm of 0.75 $Nm^3/h/m^2$. A first experiment was carried out with demineralized water without addition of media, it will be used as reference. Two other experiments were performed with the addition of inert media (beads and hollow cylinders) for a volume fraction of 0.45% v/v. The results highlight the establishment of an operating regime that stabilizes after one hour of filtration. If we consider only the measurements from one hour of filtration, in which the permeability measurement is stable. For the three experiments carried out (in the presence or absence of media) under similar operating conditions, it can be seen that the results of water filtration are practically identical (considering an error on the permeability measurement of ± 15%). It can therefore be stated that the addition of inert

media does not lead to membrane clogging since the permeability is similar with or without QQ media.

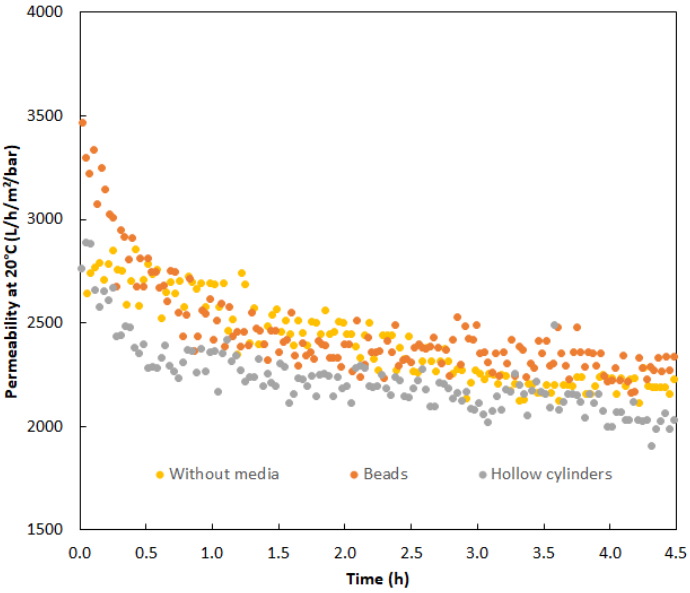

Figure 11. Evolution of the permeability of the membrane for water at 20°C with and without solid media.

4. Conclusion

In this article, an attempt has been made to quantitatively characterize the mass transfer phenomena that can be involved in the application of a bacterial antifouling technique (Quorum Quenching) using different shapes of alginate supports for bacteria for the first time in literature. Considering that the Quorum Quenching can be based on an endo-enzyme-producing bacterium or an exoenzyme-producing one, two kinds of mass transfer were distinguished for the study: liquid-solid mass transfer to mimic the transport of signal molecules from the mixed liquor to the inner part of solid media; and solid-liquid mass transfer to mimic the transport of exoenzymes from the solid media to the mixed liquor. Using a model (dye) molecule under different hydrodynamic conditions, the mass transfer kinetics characterization enabled the following main conclusions to be drawn. First, the tools selected for the characterization of the mass transfer proved to be efficient for the purpose. The experimental setups and the theoretical approaches provided relevant information about both kinds of mass transfer: the study of the liquid-solid mass transfer in jar-tests determined mass transfer coefficients in the order of magnitude of 10^{-6} m.s^{-1}. The results brought to light the fact that both sheets and the hollow cylinders can be appropriate shapes for an efficient mass transfer of AHLs from the mixed liquor to the entrapped endo-enzyme producing bacteria, in terms of transferred flux under similar hydrodynamic conditions. For the beads, the liquid-solid mass transfer was found to be less efficient because their specific shape gave the internal diffusion step more weight in the overall transfer phenomenon. The study of the solid-liquid mass transfer in the aerated ALMBR was performed under different air flowrates for the three shapes of media. The effect of the air flowrate on the mass transfer coefficient was hardly quantifiable because of the difficulty of assessing the effective exchange surface area. However, the effect of shape could be determined and the most favorable shape in terms of transferred flux appears to be sheets. In the case of exoenzyme-producing bacteria

entrapped in the solid media, the transfer of exoenzymes could be more efficient for sheets than for hollow cylinders or beads. The investigation of the two kinds of mass transfer gave interesting insights for the quorum quenching application. Actually, the mass transfer coefficient for liquid-solid transfer (in the jar-test) was found to be of the order of magnitude of 10^{-6} m.s^{-1} whereas the solid-liquid transfer (in the aerated ALMBR) was 10^{-7} m.s^{-1}. The two mass transfer coefficients are not directly comparable because they were obtained under different hydrodynamic conditions, but this indicates that mechanical stirring can provide better hydrodynamic conditions to foster mass transfer. In all the cases, the beads were found to give rise to the smallest transferred flux compared to the other two shapes. However, when the fluidized surface area S_{FM} is considered, the mass transfer coefficient for beads is greater, which means that this shape could be valuable in that case, by increasing the surface (decreasing the diameter) and increasing their fluidization (increasing the air flowrate, decreasing their diameter and/or density). These findings are of great importance because they open the way to an optimized application of quorum quenching. Finally, the development of the optical technique was revealed to be relevant to study the solid-liquid mass transfer from the solid media to the liquid phase of the aerated part of the ALMBR.

References

1. Gander, M.; Jefferson, B.; Judd, S. Aerobic MBRs for Domestic Wastewater Treatment: A Review with Cost Considerations. Sep. Purif. Technol. 2000, 18, 119–130, doi:https://doi.org/10.1016/S1383-5866(99)00056-8.
2. Melin, T.; Jefferson, B.; Bixio, D.; Thoeye, C.; Wilde, W.D.; Koning, J.D.; Graaf, J. van der; Wintgens, T. Membrane Bioreactor Technology for Wastewater Treatment and Reuse. Desalination 2006, 187, 271–282, doi:https://doi.org/10.1016/j.desal.2005.04.086.
3. Xie, Z.; Wang, S.; Shen, Y. Particle-Scale Modelling of Rapid Granular Filtration in a Dual-Media Filter. Sep. Purif. Technol. 2022, 302, 122076, doi:10.1016/j.seppur.2022.122076.
4. Liu, R.; Huang, X.; Wang, C.; Chen, L.; Qian, Y. Study on Hydraulic Characteristics in a Submerged Membrane Bioreactor Process. Process Biochem. 2000, 36, 249–254, doi:https://doi.org/10.1016/S0032-9592(00)00210-7.
5. Liu, R.; Huang, X.; Sun, Y.F.; Qian, Y. Hydrodynamic Effect on Sludge Accumulation over Membrane Surfaces in a Submerged Membrane Bioreactor. Process Biochem. 2003, 39, 157–163, doi:https://doi.org/10.1016/S0032-9592(03)00022-0.
6. Prieske, H.; Drews, A.; Kraume, M. Prediction of the Circulation Velocity in a Membrane Bioreactor. Desalination 2008, 231, 219–226, doi:https://doi.org/10.1016/j.desal.2007.12.010.
7. Yan, X.; Wu, Q.; Sun, J.; Liang, P.; Zhang, X.; Xiao, K.; Huang, X. Hydrodynamic Optimization of Membrane Bioreactor by Horizontal Geometry Modification Using Computational Fluid Dynamics. Bioresour. Technol. 2016, 200, 328–334, doi:https://doi.org/10.1016/j.biortech.2015.10.050.
8. Yan, X.; Xiao, K.; Liang, S.; Lei, T.; Liang, P.; Xue, T.; Yu, K.; Guan, J.; Huang, X. Hydraulic Optimization of Membrane Bioreactor via Baffle Modification Using Computational Fluid Dynamics. Bioresour. Technol. 2015, 175, 633–637, doi:https://doi.org/10.1016/j.biortech.2014.10.133.

9. Wu, B.; Zamani, F.; Lim, W.; Liao, D.; Wang, Y.; Liu, Y.; Chew, J.W.; Fane, A.G. Effect of Mechanical Scouring by Granular Activated Carbon (GAC) on Membrane Fouling Mitigation. Desalination 2017, 403, 80–87, doi:https://doi.org/10.1016/j.desal.2015.12.003.
10. Aslam, M.; Charfi, A.; Lesage, G.; Heran, M.; Kim, J. Membrane Bioreactors for Wastewater Treatment: A Review of Mechanical Cleaning by Scouring Agents to Control Membrane Fouling. Chem. Eng. J. 2017, 307, 897–913, doi:https://doi.org/10.1016/j.cej.2016.08.144.
11. Kim, S.-R.; Lee, K.-B.; Kim, J.-E.; Won, Y.-J.; Yeon, K.-M.; Lee, C.-H.; Lim, D.-J. Macroencapsulation of Quorum Quenching Bacteria by Polymeric Membrane Layer and Its Application to MBR for Biofouling Control. J. Membr. Sci. 2015, 473, 109–117, doi:https://doi.org/10.1016/j.memsci.2014.09.009.
12. Kim, S.-R.; Oh, H.-S.; Jo, S.-J.; Yeon, K.-M.; Lee, C.-H.; Lim, D.-J.; Lee, C.-H.; Lee, J.-K. Biofouling Control with Bead-Entrapped Quorum Quenching Bacteria in Membrane Bioreactors: Physical and Biological Effects. Environ. Sci. Technol. 2013, 47, 836–842, doi:10.1021/es303995s.
13. Köse-Mutlu, B.; Ergön-Can, T.; Koyuncu, İ.; Lee, C.-H. Quorum Quenching MBR Operations for Biofouling Control under Different Operation Conditions and Using Different Immobilization Media. Desalination Water Treat. 2016, 57, 17696–17706, doi:10.1080/19443994.2015.1086899.
14. Lee, S.; Park, S.-K.; Kwon, H.; Lee, S.H.; Lee, K.; Nahm, C.H.; Jo, S.J.; Oh, H.-S.; Park, P.-K.; Choo, K.-H.; et al. Crossing the Border between Laboratory and Field: Bacterial Quorum Quenching for Anti-Biofouling Strategy in an MBR. Environ. Sci. Technol. 2016, 50, 1788–1795, doi:10.1021/acs.est.5b04795.
15. Maqbool, T.; Khan, S.J.; Waheed, H.; Lee, C.-H.; Hashmi, I.; Iqbal, H. Membrane Biofouling Retardation and Improved Sludge Characteristics Using Quorum Quenching Bacteria in Submerged Membrane Bioreactor. J. Membr. Sci. 2015, 483, 75–83, doi:https://doi.org/10.1016/j.memsci.2015.02.011.
16. Yu, H.; Lee, K.; Zhang, X.; Choo, K.-H. In Situ versus Pre-Quorum Quenching of Microbial Signaling for Enhanced Biofouling Control in Membrane Bioreactors. J. Membr. Sci. 2019, 592, 117387, doi:https://doi.org/10.1016/j.memsci.2019.117387.
17. Li, Y.-S.; Tian, T.; Li, B.-B.; Yu, H.-Q. Longer Persistence of Quorum Quenching Bacteria over Quorum Sensing Bacteria in Aerobic Granules. Water Res. 2020, 179, 115904, doi:https://doi.org/10.1016/j.watres.2020.115904.
18. Oh, H.-S.; Yeon, K.-M.; Yang, C.-S.; Kim, S.-R.; Lee, C.-H.; Park, S.Y.; Han, J.Y.; Lee, J.-K. Control of Membrane Biofouling in MBR for Wastewater Treatment by Quorum Quenching Bacteria Encapsulated in Microporous Membrane. Environ. Sci. Technol. 2012, 46, 4877–4884, doi:10.1021/es204312u.
19. Siddiqui, M.F.; Rzechowicz, M.; Harvey, W.; Zularisam, A.W.; Anthony, G.F. Quorum Sensing Based Membrane Biofouling Control for Water Treatment: A Review. J. Water Process Eng. 2015, 7, 112–122, doi:https://doi.org/10.1016/j.jwpe.2015.06.003.
20. Siddiqui, M.F.; Sakinah, M.; Singh, L.; Zularisam, A.W. Targeting N-Acyl-Homoserine-Lactones to Mitigate Membrane Biofouling Based on Quorum Sensing Using a Biofouling Reducer. J. Biotechnol. 2012, 161, 190–197, doi:https://doi.org/10.1016/j.jbiotec.2012.06.029.
21. Bouayed, N.; Dietrich, N.; Lafforgue, C.; Lee, C.-H.; Guigui, C. Process-Oriented Review of Bacterial Quorum Quenching for Membrane Biofouling Mitigation in Membrane Bioreactors (MBRs). Membranes 2016, 6, doi:10.3390/membranes6040052.

22. Köse-Mutlu Börte, Ergön-Can Tülay, Koyuncu Ismail, Lee Chung-Hak Quorum Quenching for Effective Control of Biofouling in Membrane Bioreactor: A Comprehensive Review of Approaches, Applications, and Challenges. Environ. Eng. Res. 2019, 24, 543–558, doi:10.4491/eer.2018.380.
23. Yu, H.; Lee, K.; Zhang, X.; Choo, K.-H. Core-Shell Structured Quorum Quenching Beads for More Sustainable Anti-Biofouling in Membrane Bioreactors. Water Res. 2019, 150, 321–329, doi:https://doi.org/10.1016/j.watres.2018.11.071.
24. Iqbal, T.; Weerasekara, N.A.; Lee, K.; Choo, K.-H. Impact of Encapsulated Quorum-Quenching Bacterial Dose and Feed Type on Biofouling Control in Membrane Bioreactors. J. Environ. Eng. 2020, 146, 04019109, doi:10.1061/(ASCE)EE.1943-7870.0001640.
25. Bouayed, N.; Cavalier, A.; Lafforgue, C.; Dietrich, N.; Lee, C.-H.; Guigui, C. Hydrodynamics Characterization of the Impact of Free-Moving Particles in an Air-Lift Membrane Bioreactor. Ind. Eng. Chem. Res. 2020, 59, 7943–7954, doi:10.1021/acs.iecr.9b06749.
26. Choo, K.-H.; Park, P.-K.; Oh, H.-S. 12 - Quorum Sensing and Quorum Quenching in Membrane Bioreactors. In Current Developments in Biotechnology and Bioengineering; Ng, H.Y., Ng, T.C.A., Ngo, H.H., Mannina, G., Pandey, A., Eds.; Elsevier, 2020; pp. 245–274 ISBN 978-0-12-819809-4.
27. Liu, J.; Eng, C.Y.; Ho, J.S.; Chong, T.H.; Wang, L.; Zhang, P.; Zhou, Y. Quorum Quenching in Anaerobic Membrane Bioreactor for Fouling Control. Water Res. 2019, 156, 159–167, doi:https://doi.org/10.1016/j.watres.2019.03.029.
28. Jiang, B.; Zeng, Q.; Hou, Y.; Liu, J.; Xu, J.; Li, H.; Du, C.; Shi, S.; Ma, F. Quorum Quenching Bacteria Bioaugmented GO/PPy Modified Membrane in EMBR for Membrane Antifouling. Sci. Total Environ. 2020, 718, 137412, doi:https://doi.org/10.1016/j.scitotenv.2020.137412.
29. Dietrich, N.; Jimenez, M.; Xie, X.; Hébrard, G. Optical Techniques to Evaluate Hydrodynamics and Mass Transfer in Biorectors. 2015.
30. Dietrich, N.; Loubière, K.; Jimenez, M.; Hébrard, G.; Gourdon, C. A New Direct Technique for Visualizing and Measuring Gas–Liquid Mass Transfer around Bubbles Moving in a Straight Millimetric Square Channel. Chem. Eng. Sci. 2013, 100, 172–182, doi:https://doi.org/10.1016/j.ces.2013.03.041.
31. Xu, F.; Hébrard, G.; Dietrich, N. Comparison of Three Different Techniques for Gas-Liquid Mass Transfer Visualization. Int. J. Heat Mass Transf. 2020, 150, 119261, doi:https://doi.org/10.1016/j.ijheatmasstransfer.2019.119261.
32. Oh, H.-S.; Kim, S.-R.; Cheong, W.-S.; Lee, C.-H.; Lee, J.-K. Biofouling Inhibition in MBR by Rhodococcus Sp. BH4 Isolated from Real MBR Plant. Appl. Microbiol. Biotechnol. 2013, 97, 10223–10231, doi:10.1007/s00253-013-4933-7.
33. Wang, J.; Quan, C.; Wang, X.; Zhao, P.; Fan, S. Extraction, Purification and Identification of Bacterial Signal Molecules Based on N-Acyl Homoserine Lactones. Microb. Biotechnol. 2011, 4, 479–490, doi:https://doi.org/10.1111/j.1751-7915.2010.00197.x.
34. Yuh-Shan, H. Citation Review of Lagergren Kinetic Rate Equation on Adsorption Reactions. Scientometrics 2004, 59, 171–177, doi:10.1023/B:SCIE.0000013305.99473.cf.
35. Wu, F.-C.; Tseng, R.-L.; Huang, S.-C.; Juang, R.-S. Characteristics of Pseudo-Second-Order Kinetic Model for Liquid-Phase Adsorption: A Mini-Review. Chem. Eng. J. 2009, 151, 1–9, doi:https://doi.org/10.1016/j.cej.2009.02.024.
36. Furusawa, T.; Smith, J.M. Fluid-Particle and Intraparticle Mass Transport Rates in Slurries. Ind. Eng. Chem. Fundam. 1973, 12, 197–203, doi:10.1021/i160046a009.

37. Dotto, G.L.; Moura, J.M.; Cadaval, T.R.S.; Pinto, L.A.A. Application of Chitosan Films for the Removal of Food Dyes from Aqueous Solutions by Adsorption. Chem. Eng. J. 2013, 214, 8–16, doi:10.1016/j.cej.2012.10.027.
38. Dotto, G.L.; Buriol, C.; Pinto, L.A.A. Diffusional Mass Transfer Model for the Adsorption of Food Dyes on Chitosan Films. Chem. Eng. Res. Des. 2014, 92, 2324–2332, doi:https://doi.org/10.1016/j.cherd.2014.03.013.
39. Sänger, P.; Deckwer, W.-D. Liquid—Solid Mass Transfer in Aerated Suspensions. Chem. Eng. J. 1981, 22, 179–186, doi:10.1016/0300-9467(81)80013-5.
40. Noyes, A.A.; Whitney, W.R. THE RATE OF SOLUTION OF SOLID SUBSTANCES IN THEIR OWN SOLUTIONS. J. Am. Chem. Soc. 1897, 19, 930–934, doi:10.1021/ja02086a003.